analytical chemistry

Article

Cite This: Anal. Chem. 2017, 89, 11672-11678

pubs.acs.org/ac

Reconceptualizing Fluorescence Correlation Spectroscopy for Monitoring and Analyzing Periodically Passing Objects

Eli Zamir,*,† Christoph Frey,† Marian Weiss, Silvia Antona, Johannes P. Frohnmayer, Jan-Willi Janiesch, Ilia Platzman, and Joachim P. Spatz*

Department of Cellular Biophysics, Max Planck Institute for Medical Research, Jahnstraße 29, D-69120 Heidelberg, Germany
Department of Biophysical Chemistry, University of Heidelberg, Im Neuenheimer Feld 253, D-69120 Heidelberg, Germany

Supporting Information

ABSTRACT: Fluorescence correlation spectroscopy (FCS) is a sensitive technique commonly applied for studying the dynamics of nanoscale-labeled objects in solution. Current analysis of FCS data is largely based on the assumption that the labeled objects are stochastically displaced due to Brownian motion. However, this assumption is often invalid for microscale objects, since the motion of these objects is dominated by Stokes drag and settling or rising effects, rather than stochastic Brownian motion. To utilize the power of FCS for systems with nonstochastic displacements of objects, the collection and analysis of FCS data have to be reconceptualized. Here, we extended the applicability of FCS for the detection and analysis of periodically passing objects. Toward this end, we implemented droplet-based microfluidics, in which monodispersed droplets containing fluorescent marker are flowing equally spaced within microchannels. We show by simulations and experiments that FCS can sensitively quantify the flow-rates, variability, and content of rapidly passing droplets. This information can be derived at high temporal resolution, based on the intensity fluctuations generated by only 5−10 passing droplets. Moreover, by utilizing the periodicity of the flowing droplets for noise reduction by averaging, FCS can monitor accurately the droplets flow even if their fluorescence intensity is negligible. Hence, extending FCS for periodically passing objects converts it into a powerful analytical tool for high-throughput droplet-based microfluidics. Moreover, based on the principles described here, FCS can be straightforwardly applied for a variety of systems in which the passing of objects is periodic rather than stochastic.

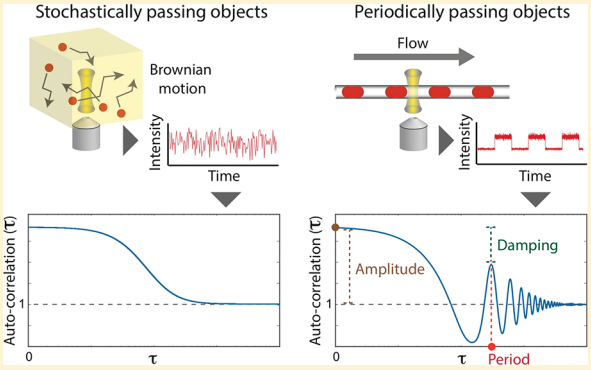

Fluorescence correlation spectroscopy (FCS) derives information from the temporal fluctuations of fluorescence intensity.[1−5] By sensitive high-rate sampling, typically >10 MHz, FCS records the intensity fluctuations generated by labeled particles passing through an observed confocal volume within the sample. The fundamental analysis of FCS data is the autocorrelation function $G(\tau)$—calculated as the correlation of the recorded intensity trace with a delayed copy of itself as a function of the delay, τ.[1] FCS is commonly applied for studying nanoscale objects (e.g., small molecules,[6] proteins,[1] quantum dots,[7] and liposomes[8]) passing the observed volume stochastically due to diffusion and flow.[1,5,9] Accordingly, the interpretations of $G(\tau)$ relies largely on the assumption that the labeled particles are been stochastically displaced due to Brownian motion.[10] Such stochasticity implies that the number of particles present in the confocal volume at the different time points distributes in a Poisson manner. Since for a Poisson distribution the variance is equal to the mean, the concentration of the labeled particles can be inferred from the amplitude of the autocorrelation. Additionally, the stochastic particles displacement implies that $G(\tau)$ decays as a function of τ, gradually approaching a baseline corresponding to zero correlation. The decay of $G(\tau)$ reflects the gradual and independent entry and exit of labeled particles in the observed volume. Accordingly, from this decay, the mobility mechanism of the particles and its parameters, such as diffusion and flow speeds, can be inferred. However, while these implications are based on the stochastic displacements of nanoscale objects in solution, a large variety of fluid dynamic processes involve motion of microscale objects. For microscale objects, Brownian motion is much less prominent, while nonstochastic displacement mechanisms dominated by Stokes drag in a laminar flow and gravity are more prevailing. Moreover, acoustic waves and electromagnetic fields can affect the displacements of microscale objects nonstochastically and arrange them in spatial patterns. To extend the applicability of FCS for such nonstochastic systems, its analysis has to be reconceptualized.

One type of nonstochastic displacements is a constant flow of equally spaced objects. Such a flow mode is typical in droplet-based microfluidics. This technology generates via

Received: August 3, 2017
Accepted: October 6, 2017
Published: October 6, 2017

DOI: 10.1021/acs.analchem.7b03108
Anal. Chem. 2017, 89, 11672−11678

microchannels picoliter-scale monodisperse emulsion droplets at rates ranging from a slow drip to over 1 MHz.[11−15] The detection of droplets and their content is based mainly on fluorescence, due to the relatively high sampling rate and sensitivity of photodetectors. Conventionally, this detection relies on identifying the single droplets along the trace by segmentation using intensity threshold and/or other object-recognition criteria.[16−19] This makes the monitoring of droplets dependent on assumptions, manual tuning of parameters, and dedicated segmentation algorithms. Additionally, accurate segmentation of droplet depends on having a sufficient fluorescence signal of each droplet in comparison to the background fluorescence in the gaps between the droplets. Therefore, despite the progress made in recent years, sensitive and rapid monitoring tools are needed to further facilitate high-throughput applications of droplet-based microfluidics.[20,21]

In this work, we extended the applicability of FCS for the study of periodically passing objects. We demonstrate that this extension converts FCS into a powerful detection method for droplet-based microfluidics, enabling us to monitor rapidly and sensitively the flow and content of passing droplets.

MATERIALS AND METHODS

Production of Microfluidic Devices. The microfluidic devices (Figure S1) were designed with QCAD-pro (Ribbon-Soft, Switzerland). Photomasks were printed on chrome-coated soda lime glass (JD-Photodata, U.K.). For the photolithography process, a negative photoresist (SU8−3025, MicroChem, U.S.A.) was spin-coated (Laurell Technologies Corp., U.S.A.) onto silicon wafers at 2500 rpm in order to get a uniform coating of 30 μm thickness. Wafers were then placed on a hot plate for a 5 min soft bake at 65 °C, then ramped slowly to 95 °C and held for 15 min. Following this, the photoresist was exposed for 7.5 s to UV light through the corresponding photomask using a mask aligner (MJB4, SÜSS MicroTec, Germany). For the post-exposure bake, the wafers were placed for 1 min on a hot plate at 65 °C and 5 min at 95 °C. The remaining resist was removed with mr-DEV 600 developer (MicroChemicals, Germany). The hard bake was carried out in an oven at 150 °C for 15 min. Soft lithography was performed as previously described.[22,23] Briefly, polydimethylsiloxane (PDMS; Sylgard 184, Dow Corning, U.S.A.) was prepared by mixing the oligomer with the polymerization catalyst in a 9:1 (w/w) ratio. The mixed, degassed elastomer was poured over the silicon wafer and cured at 65 °C for 2 h in the oven. After curing, the flexible PDMS mold was peeled off the wafer and injection holes with a diameter of 0.75 mm were punched (Biopsy Punch, World Precision Instruments, U.S.A.). The device was cleaned with ethanol and activated together with a 24 × 60 mm coverslip (#1, Carl Roth, Germany) in an oxygen plasma (PVA TePla 100, PVA TePla, Germany; 0.45 mbar, 200 W, 20 s).[24] After activation, the PDMS device was pressed on the coverslip and heated for at least 2 h at 65 °C. Sigmacote (Sigma-Aldrich, Germany) was applied to the microchannels of the device in order to make their surfaces hydrophobic.

Surfactant Synthesis. Following a previously published protocol,[25,26] the synthesis of the PFPE (7000 g/mol)-PEG (1400 g/mol)-PFPE (7000 g/mol) triblock copolymer was carried out under argon atmosphere in dry THF solvent (tetrahydrofuran, 99.8%, Carl Roth, Germany) in a heated Schlenk-flask. First, 1 mmol PEG (1400 mg, 1400 g/mol molecular weight, Sigma-Aldrich, Germany) was dissolved in 90 mL of dry THF and cooled to −78 °C. At this temperature, 1.25 mL of *N*-butyl lithium (1.6 M solution in hexane, 2 mmol, Sigma-Aldrich, Germany) was added dropwise over 1 h and stirred for additional 30 min. Under continuous stirring, the reaction was slowly heated to room temperature and stirred for another 30 min. Then, 14 g of Krytox FSH (PFPE-carboxylic acid, 2 mmol, 7000 g/mol molecular weight, DuPont, Netherlands) was added dropwise over 30 min and stirred for 2 h. THF solvent with unreacted PEG was removed by a separatory funnel. After two THF washing steps, the product was dissolved in methanol (99.8%, Carl Roth GmbH, Germany) and dried with a rotary evaporator at 40 °C. The quality of the synthesized surfactant was analyzed by NMR and FT-IR measurements.

Droplet Production. For stable production of water-in-oil droplets,[27−29] a 5 mM solution of PFPE (7000 g/mol)-PEG (1400 g/mol)-PFPE (7000 g/mol) in HFE-7500 oil (3M, U.S.A.) was used as the oil phase. The aqueous phase consisted of PBS with 2 μM, 20 nM, or 2 nM Alexa Fluor 647 (C2-maleimide, A20347, Molecular Probes) as indicated. Different droplet production frequencies, between ∼2−20 kHz, were generated by adjusting the flow rates of the aqueous and oil phases ranging from 400 to 1000 μL/h and 800 to 3000 μL/h, respectively (Supplementary Table S1). All fluids were injected into the microfluidic device using 1 mL syringes (Omnifix-F, B. Braun Melsungen AG, Germany) connected by a cannula (Sterican, 0.4 × 20 mm, BL/LB, B. Braun) and PTFE-tubing (0.4 × 0.9 mm, Bola, Germany). For a fine flow-control, syringe pumps (Pump11Elite, Harvard Apparatus, U.S.A.) were used. High-speed camera (Phantom 7.2, Vision Research, U.S.A.) was used for a visual quality assessment of droplets production.

Encapsulation of Cells. CHO suspension cells were cultured in growth medium (EX-CELL ACF DHO Medium, Sigma-Aldrich, Germany) enriched with 4 mM solution of L-Glutamine (Gibco, ThermoFisher, U.S.A.). Prior to encapsulation, the cells were centrifuged for 5 min at 700 rpm and resuspended in PBS containing 8 μM Hoechst 33342 (Trihydrochloride, ThermoFisher, U.S.A.). Following an incubation of 10 min, the cells were washed three times by centrifugation and resuspension with PBS. Finally, the cells were suspended in PBS containing 2 μM Alexa Fluor 647 (C2-maleimide, A20347, Molecular Probes) to a concentration of 40 million cells per ml.

Microscopy. Fluorescence intensity measurements of flowing droplets were carried out on a LSM 880 confocal microscope (Carl Zeiss, Germany), using a C-Apochromat 40 × /1.2 W water-immersion objective (Carl Zeiss, Germany). Samples were excited with 405 and 633 nm laser lines, and fluorescence emission was detected within 419−615 nm and within 650−695 nm for the green and red detection channel, respectively. The pinhole was fully opened, to maximize photon collection and minimize optical sectioning. Photon count rate was detected and recorded at a sampling rate of 15 MHz.

Data Analysis. Autocorrelation curves of the acquired FCS data were calculated using the LSM software (ZEN, Carl Zeiss, Germany) in parallel with the data acquisition. For further analyses, the ConfoCor3 raw data files, listing time intervals between detected photons, were converted using a C++ program to ASCII files indicating the number of photons detected during each time bin (here 1 μs) along the measurement—hence obtaining $F_D(t)$ and $F_C(t)$. Where indicated, the single droplets were identified along $F_D(t)$ by segmentation, as described in the text. To segment encapsulated cells within each droplet, $F_C(t)$ fragments

DOI: 10.1021/acs.analchem.7b03108
Anal. Chem. 2017, 89, 11672−11678

corresponding to passing droplets were subjected to a modified one-dimensional watershed algorithm. The analyses of $F_D(t)$ and $F_C(t)$, and the autocorrelation of simulated $F_D(t)$ traces, were done with Matlab (Mathworks, U.S.A.).

Simulations. Simulations of intensity traces of flowing droplets were performed to systematically assess the derivation of droplets flow and content parameters from the autocorrelation curve. The input parameters for the simulation included the average fluorescence intensity level within a droplet (Fd) and in the gap between droplets (Fg), the average passing time of the droplets in the microfluidic channel (Ld), the average passing time of the gap between each two sequential droplets (Lg) and the variance of the droplet and gap passing times (noise, Dn). The intensity value in each time point within a droplet segment and within a gap segment was sampled from a Poisson distribution having a mean value of Fd and Fg, respectively. The time point at which a droplet segment ends, in respect to its start point, was sampled from a normal distribution having a mean value of Ld and a standard deviation of Dn. Similarly, the time point at which a gap segment ends, in respect to its start point, was sampled from a normal distribution having a mean value of Lg and a standard deviation of Dn. All simulations were done in Matlab (Mathworks, U.S.A.).

RESULTS AND DISCUSSION

Interpreting the Autocorrelation of Periodically Passing Objects. The autocorrelation function, $G(\tau)$, of the recorded fluorescence intensity fluctuation trace $F(t)$ can be written as $G(\tau) = \langle \delta F(t) \cdot \delta F(t+\tau) \rangle / \langle F(t) \rangle^2 + 1$, where $\delta F(t) = F(t) - \langle F(t) \rangle$. While the derivation of $G(\tau)$ from $F(t)$ is a straightforward calculation, the interpretation of $G(\tau)$ depends on the mechanisms underlying the fluorescence fluctuations. In the case of droplet flow, fluctuations along the intensity trace of the droplet marker, $F_D(t)$, are caused mainly by the constant flow of periodically passing droplets (Figure 1A and Figure S2). This periodicity in $F_D(t)$ is manifested by oscillations in $G_D(\tau)$ (Figure 1B).

We identified several important parameters concerning the droplets flow and content that can be derived from the autocorrelation curve $G_D(\tau)$ (Figure 1B):

(1) The τ value τ_{fp}, at which $G_D(\tau)$ reaches the first oscillation peak, indicates the average time period that is needed for a droplet and its subsequent gap to fully pass the observed volume. Hence, $1/\tau_{fp}$ equals the flow rate of the droplets (i.e., the number of droplets passing per time interval).

(2) In the case of homogeneous droplets and gaps, $G_D(\tau_{fp})$ should be equal to the amplitude of the autocorrelation curve, $G_D(0)$. Variation in droplets or gap sizes would cause damping of the $G_D(\tau)$ oscillations, allowing the quantification of irregularities in the flow of droplets, for example as $1 - G_D(\tau_{fp})/G_D(0)$.

(3) The autocorrelation amplitude, $G_D(0)$, equals to $\langle F_D(t)^2 \rangle / \langle F_D(t) \rangle^2$ (Supplementary Note S1). This implies that for homogeneously labeled droplets, $G_D(0) = P_D(1 - P_D)(\gamma - 1)^2/(1 + P_D(\gamma - 1))^2 + 1$, where P_D = (mean droplet passing time)$/\tau_{fp}$ and γ is the ratio of droplets intensity over the background fluorescence intensity in the gaps between droplets (Supplementary Note S1). The partial derivative of $G_D(0)$ with respect to γ is positive, hence for a given P_D value, a higher autocorrelation amplitude implies a higher droplets intensity (Supplementary Note S1), given $\gamma > 1$. Thus, the autocorrelation amplitude provides a handle to monitor changes in droplets fluorescence intensity due to biological or chemical processes.

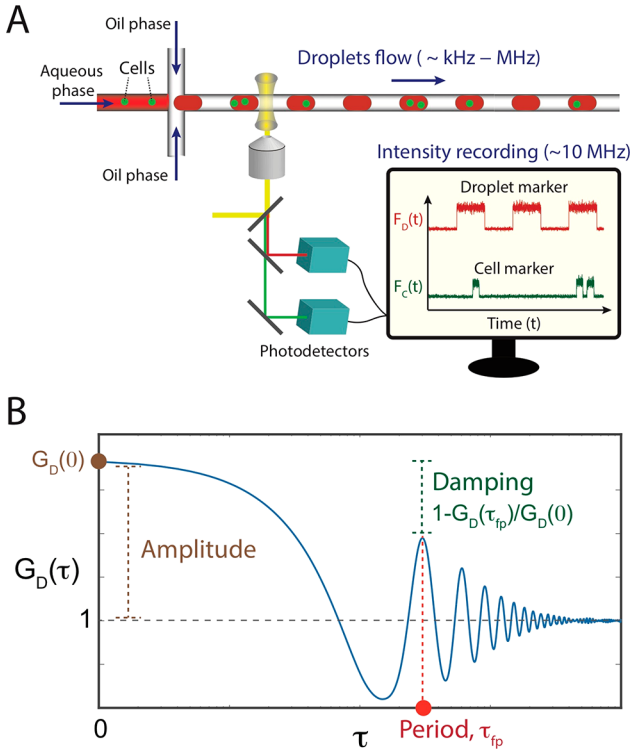

Figure 1. FCS-based monitoring of droplet flow and content in high-throughput microfluidics. (A) Schematic representation of a flow-focusing junction, where cell-containing droplets are generated, and of the FCS-based detection setup. Intensity fluctuations of a droplet marker, $F_D(t)$, and a cell marker, $F_C(t)$, are recorded at high sampling rates (15 MHz) at a spot along a droplet-carrying microchannel. (B) The autocorrelation curve of the droplet marker, $G_D(\tau)$, is calculated instantaneously. From this curve, the following parameters can be derived: (1) the period of $G_D(\tau)$ oscillations, τ_{fp} equals to 1/(droplet flow rate), (2) the extent of damping in $G_D(\tau)$ oscillations indicates the variability of droplets size or speed, (3) the amplitude of $G_D(\tau)$ can indicate changes in the (mean droplets fluorescence intensity)/(mean gaps fluorescence intensity) ratio.

Simulation Assessments of Autocorrelation Responses to Droplet Parameters. We first assessed by simulations of droplet-marker intensity traces, $F_D(t)$, the effects of droplet flow and intensity on the autocorrelation curve $G_D(\tau)$ (Figure 2). The results show that droplet flow rates ranging from 20 Hz–5 MHz were accurately inferred from the $1/\tau_{fp}$ of the autocorrelation curve, given $F_D(t)$ with a temporal resolution of 0.1 μs (Figure 2, left column, upper row). Hence, autocorrelation can capture correctly the maximum theoretically feasible frequency, the Nyquist frequency, for a given sampling rate.

The large changes in droplet flow rates, up to ~2.5 MHz, did not affect the damping extent and the amplitude of $G_D(\tau)$-(Figure 2, left column). At 5 MHz, the damping extent of $G_D(\tau)$ decreased, reflecting under-sampling of the passing-time and intensity of each single droplet. Changing the standard deviation of the passing times of the droplets and gaps from 0 to 0.3 caused linearly proportional changes in the damping

DOI: 10.1021/acs.analchem.7b03108
Anal. Chem. 2017, 89, 11672–11678

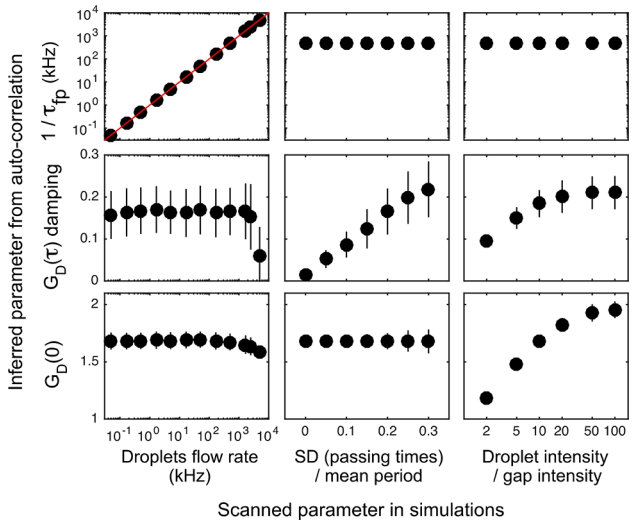

Figure 2. Simulation-based assessment of the effects of droplet flow parameters on the autocorrelation curve $G_D(\tau)$. Intensity fluctuation traces of flowing droplets, $F_D(t)$, were simulated as described. The default flow parameters were the following: intensity trace time resolution = 0.1 μs (corresponding to a sampling rate of 10 MHz), mean droplet passing time = 1 μs, mean gap passing time = 1 μs (resulting a flow rate of 500 kHz), standard deviation (SD) of droplet and gap passing time = 20% of the mean passing time, gap mean fluorescence intensity = 10 (a.u.), droplet mean fluorescence intensity = 100 (a.u.). The length of the simulated $F_D(t)$ spanned 5 passing droplets for the left and middle columns, and 15 passing droplets for the right column. Each column in the graph panel corresponds to a given simulation parameter that was altered. The ratio between the mean droplets intensity and mean gaps intensity was altered by changing the former one. Each row in the graph panel corresponds to a given parameter that was inferred from the autocorrelation curve $G_D(\tau)$. The damping of $G_D(\tau)$ was calculated as $1 - G_D(\tau_{fp})/G_D(0)$. Error bars indicate standard deviation (n = 300 simulation repeats).

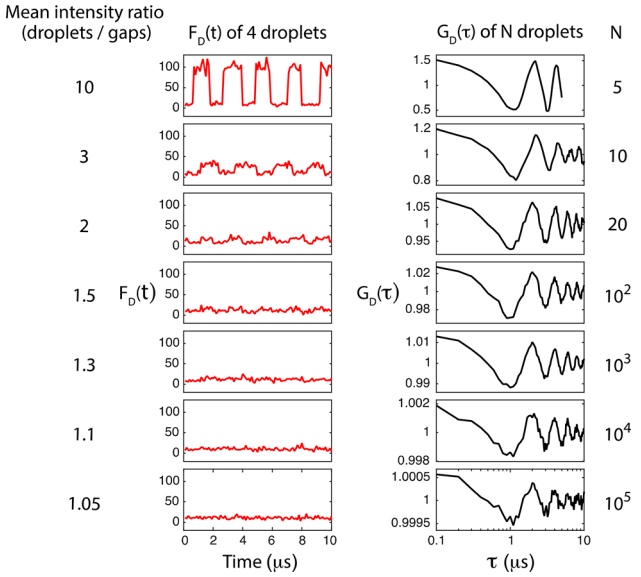

Figure 3. Autocorrelation captures the flow rates of droplets even with marginal fluorescence intensity. Intensity fluctuation traces of flowing droplets, $F_D(t)$, were simulated as described. The flow parameters were the following: intensity trace time resolution = 0.1 μs, mean droplet passing time = 1 μs, mean gap passing time = 1 μs (resulting a flow rate of 500 kHz), standard deviation of droplet and gap passing time = 20% of the mean passing time, mean gap fluorescence intensity = 10. The mean droplets fluorescence intensity was varied to achieve different ratios with the mean gap intensity, as indicated. The plots on the left show the simulated $F_D(t)$ for the first 10 μs, during which 4 droplets are fully passing. The plots on the right show the autocorrelation curves, $G_D(\tau)$, obtained from the corresponding $F_D(t)$ spanning the indicated number of passing droplets (N).

extent of $G_D(\tau)$, without changing $G_D(0)$ or $1/\tau_{fp}$ (Figure 2, middle column).

Changing the ratio of the droplets intensity over the background intensity in the gaps from 2 to 100 increased $G_D(0)$ (Figure 2, right column, bottom row). As expected, at high droplet/gap intensity ratio $G_D(0)$ converges to $1+(1 - P_D)/P_D$ (here, equals to 2), where P_D (here 0.5) equals (mean droplet passing time)/(mean droplet + gap passing time) (Supplementary Note S1). Increase of the droplet/gap intensity ratio also enhanced the damping extent of $G_D(\tau)$ but did not affect τ_{fp} (Figure 2, right column).

Conventionally, the monitoring of flowing droplets in microfluidics is performed in the time domain (i.e., by recognizing each droplet as an object along the recorded temporal intensity fluctuation trace).[16−19] Such recognition requires to have a sufficient signal-to-noise ratio of the labeled droplets to overcome stochastic fluctuations of intensity. Moreover, high droplet flow rates reduce the sampling points for each passing droplet, and hence reduce the statistical confidence in identifying and distinguishing the single droplets. In contrast to time-domain based analyses, autocorrelation captures and integrates the periodicity of a signal. Therefore, even if the fluorescence signal of the droplets is marginal, autocorrelation can be expected to capture their flow by integrating a sufficient number of droplets. We first assessed this expectation by simulating intensity traces of droplets flowing at 500 kHz rate with different (mean droplets intensity)/(mean gap intensity) ratios (Figure 3). The intensity of the droplets and gaps at each time bin was sampled from a Poisson distribution around the mean droplets intensity and the mean gaps intensity, respectively. At droplet/gap intensity ratio ≤2, it is practically impossible to identify the single droplets along the intensify traces (Figure 3, left column). Remarkably, autocorrelation clearly detected the flow of droplets and accurately quantified its rate, even at droplet/gap intensity ratio of 1.05 (Figure 3, right column). At droplet/gap intensity ratio of 2, only 20 droplets were needed to be integrated by autocorrelation for a clear quantification of their flow rate. At the marginal droplet/gap intensity ratio of 1.05, the integration power of autocorrelation utilized 100 000 droplets passing during 0.2 s to clearly capture their flow rate.

To conclude, the simulation assessments indicate that the autocorrelation curve $G_D(\tau)$ can (1) quantify accurately fast droplet flow rates, up to the maximum theoretically possible for a given sampling rate, (2) provide a quantitative measure for changes in the variability of the droplets and gaps passing times, and (3) provide a quantitative measure for changes in the droplets' intensity/gap intensity ratio, for a given droplet-flow condition. Given a sufficient fluorescence intensity of droplets, it is enough to use short intensity traces, spanning the mean passing time of 5−10 droplets, to achieve accurately these quantifications. Additionally, the simulations show that even with a negligible droplets fluorescence intensity, the autocorrelation can accurately monitor and characterize their flow, by integrating the signal over a larger number of droplets.

DOI: 10.1021/acs.analchem.7b03108
Anal. Chem. 2017, 89, 11672−11678

Experimental Assessment of Droplet Monitoring by FCS. Following the assessment by simulations, we tested experimentally the effects of droplet flow conditions on the autocorrelation curve $G_D(\tau)$. First, we produced droplets containing 2 μM Alexa Fluor 647 at different rates (Figure 4A and Figure S3) and measured their flow rates by autocorrelation (Figure 4B). FCS data acquisition of the stream of droplets was performed at a spot adjacent to the flow-focusing junction (Figure 1A). Autocorrelation analysis of the recorded intensity traces shows that the values of τ_{fp} get smaller as the input flow rates increase, hence indicating a higher droplet flow rate (Figure 4B). As a quantitative control, short time-lapse movies (~300 ms) were recorded using a high-speed camera, and the number of passing droplets per time period was counted (Figure S3 and Table S1). The droplet flow rates obtained from direct counting matched well those obtained from autocorrelation analysis (Figure 4C). Hence, these results confirmed the capability of autocorrelation to monitor accurately droplet flow rates.

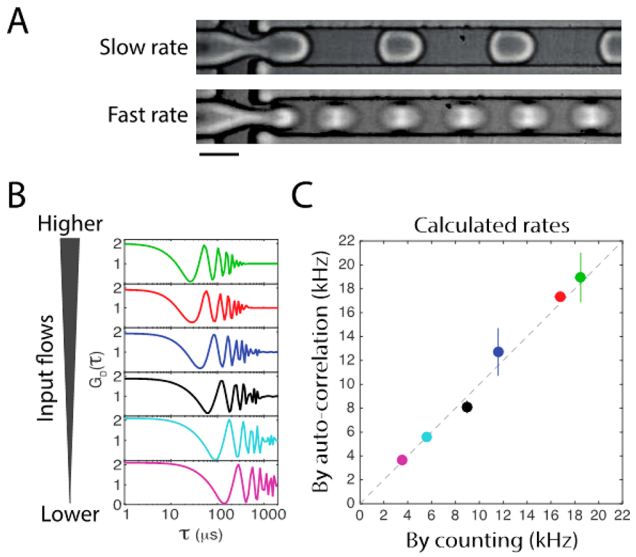

Figure 4. Accurate quantification of droplet flow rates by autocorrelation. Droplets were generated at different rates by modifying the input flow rates of the aqueous and oil phases, as indicated in Supplementary Table S1. (A) High-speed camera transmission images of droplets generated at the lowest (Slow rate) and highest (Fast rate) applied rates (Supplementary Table S1). Scale bar, 30 μm. (B) The autocorrelation, $G_D(\tau)$, curves obtained for different rates of droplet flow. (C) A scatter plot comparing the quantifications of droplet flow rates by autocorrelation and direct droplet counting. Dashed line indicates the line of equality. Error bars indicate the standard deviation ($n = 6$ and $n \geq 3$ for the horizontal and vertical axes, respectively). The color-code matches each data point in (C) with the corresponding example of autocorrelation curve in (B).

Next, we experimentally tested the effect of inhomogeneity in the droplet flow on the autocorrelation curve $G_D(\tau)$. By high-speed camera imaging, we noticed that cell encapsulation affects the speed of the encapsulating droplets, hence increases the variability of the distances between passing droplets (Figure 5A). Therefore, cell encapsulation provides an experimental system to induce droplet-flow inhomogeneity, which is relevant for many potential microfluidic applications. In order to generate flow variability, we added Hoechst-labeled cells into the input aqueous phase, leading to encapsulation of cells in the forming droplets (Figure 1A). At the applied droplet production rate (~20 kHz), cell encapsulation affected the speed of cell-containing droplets (Figure 5A). To study the effect of induced inhomogeneous droplet flow on $G_D(\tau)$ the density of cells was adjusted so that encapsulations were occurring stochastically. As predicted, the damping of $G_D(\tau)$ oscillations was found to be much stronger for the sessions of droplet production which included encapsulation of cells (Figure 5B,C).

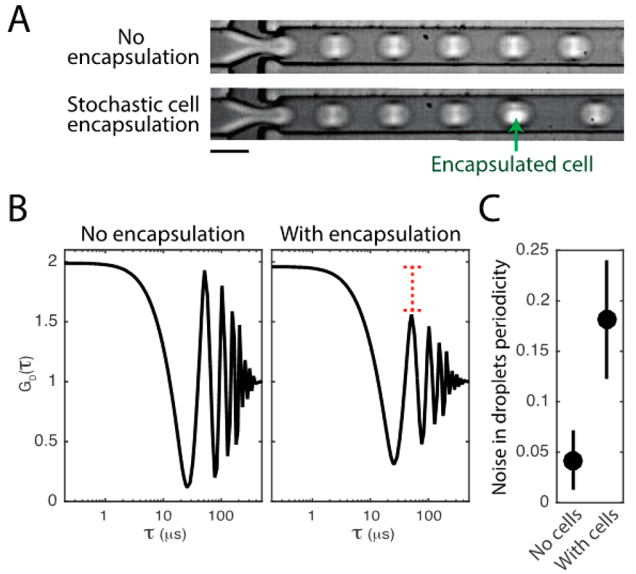

Figure 5. Quantifying the variability of droplet passing time by autocorrelation. $F_D(t)$ was recorded for droplets produced with or without cells encapsulation. (A) High-speed camera transmission images of droplets generated with or without stochastic encapsulation of cells. Scale bar, 30 μm. (B) Representative autocorrelation curves obtained with or without cells encapsulation. (C) A plot showing the mean ± standard deviation of the inferred level of periodicity noise, calculated as $1 - G_D(\tau_{fp})/G_D(0)$. Error bars indicate standard deviation ($n \geq 6$).

In order to experimentally assess the effects of droplet/gap intensity ratios on $G_D(\tau)$, we produced droplets containing different concentrations of the fluorescent marker. As expected, the results show that for given flow conditions and excitation intensity, the autocorrelation amplitude $G_D(0)$ decreases as the droplets intensity decreases (Figure 6A). Remarkably, the autocorrelation provided an accurate measure of the droplet flow rates even if their fluorescence intensity is marginal (Figure 6A, 2 nM marker concentration). Moreover, autocorrelation captures the flow of droplets and its rate even if the droplets are unlabeled (Figure 6B). This sensitive detection is possible since autocorrelation averages negligible, periodic, changes of intensity levels generated as droplets are passing through the observed volume. The intensity changes are due to autofluorescence of the oil phase, which is marginal but still higher in comparison with the aqueous phase (Figure S4). Since averaging reduces the random noise, but not the mean fluorescence difference between droplets and gaps, autocorrelation increases the signal-to-noise ratio. Of note, autofluorescence of the oil phase is an important factor to account for, if its level is comparable to, or higher than, the fluorescence signal of the droplets. Particularly, if the fluorescence signal of the droplets is lower than the oil autofluorescence, $G_D(0)$ will be lower than that of droplets with no fluorescence signal.

DOI: 10.1021/acs.analchem.7b03108
Anal. Chem. 2017, 89, 11672−11678

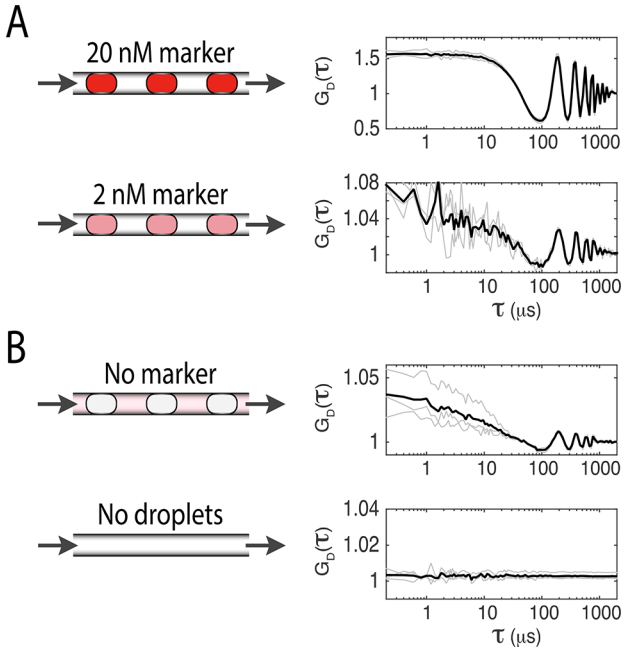

Figure 6. Effect of droplets relative fluorescence intensity on their autocorrelation curve. (A) Droplets were generated under the same flow conditions, with aqueous phase containing a fluorescent marker (Alexa 647) at 20 nM or 2 nM in PBS, as indicated. The autocorrelation curves $G_D(\tau)$ obtained for each measurement repeat of 10 s (thin lines) and their average (thick line, n = 3) are shown. (B) Autocorrelation curves and their averages (n = 3) of droplets containing PBS alone, or of flowing PBS without droplets formation (due to lack of oil-phase flow into the cross-junction). In (A) and (B) samples were excited solely with laser line 633 nm, and with power attenuator set to 0.3% power for (A) and to 30% power for (B). In the case of high laser power, a marginal autofluorescence of the oil phase can be detected, enabling to monitor flowing droplets containing no fluorescence marker. Thin and thick curves correspond to the measurement repeats and their mean, respectively.

Therefore, when dealing with marginal fluorescence signals it is important to measure the $G_D(0)$ of droplets containing no marker and calibrate accordingly.

Temporal Resolution of Droplet Monitoring by FCS. To provide a real-time feedback for rapid changes in a periodic flow of objects, the autocorrelation analysis should enable to derive information from short segments of the intensity trace $F_D(t)$. The simulation analysis indicated that given sufficient intensity, only few droplets are needed to be integrated to enable their flow-rate detection (Figure 3). To test this using experimental data, we applied multiresolution FCS (mrFCS)[7] analysis, scanning the recorded intensity fluctuation traces with different temporal integration levels. Toward this end, we partitioned $F_D(t)$ to short time periods (ranging from 200 to 2000 μs) and calculated $G_D(\tau)$ for each period along the trace. Analysis of a 500 μs period (5−10 droplets) was found to be sufficient for detecting an inhomogeneity in the droplet flow (Figure S5). Thus, by scanning $F_D(t)$ with a sliding window, and calculating $G_D(\tau)$ per each window, it is possible to monitor the cell-encapsulation frequency at a temporal resolution of 500 μs, corresponding to 5−10 passing droplets (Figure S5).

In addition to $G_D(\tau)$, the amplitude of the cell-marker autocorrelation, $G_C(\tau)$, can be calculated for each short time interval (Figure S5). In the absence of encapsulated cells the amplitude of $G_C(\tau)$, $G_C(0)$, is low, due to uncorrelated intensity fluctuations and weakly labeled small debris. In the presence of one or more encapsulated cells $G_C(0)$ increases considerably, since the cells are few in number, relatively big and strongly labeled. Thus, $G_C(\tau)$ and $G_D(\tau)$ provide two independent indicators for cell encapsulation.

Identifying Objects within Flowing Droplets via FCS Data Acquisition. FCS relies on having fast sampling rates, typically >10 MHz, in order to capture accurately the residence time of diffusing particles in the confocal volume. This provides high spatial resolution for resolving signals of encapsulated cells or other objects within fast flowing droplets (Figure 1A and Figure S2). Segmentation of the droplets along $F_D(t)$ identifies the start and end of each droplet along the trace, hence enables analyzing its content along the corresponding part of the cell-marker intensity trace $F_C(t)$ (Figures S6 and S7). Thus, encapsulated cells within each flowing droplet can be detected and counted by segmenting them along the corresponding $F_C(t)$ fragment (Figure S8).

CONCLUSIONS

This study shows that FCS can be effectively applied for the study of periodically passing objects. To achieve this goal, we reconfigured the manner by which the autocorrelation is interpreted and analyzed. Moreover, we demonstrated that this approach converts FCS into a sensitive analytical tool for monitoring flowing droplets and their content in microfluidic devices. We showed that, in contrast to segmentation-based methods, autocorrelation can monitor and quantify ultrafast droplet flow rates accurately, even with very faint fluorescence signals. Additionally, FCS can monitor the heterogeneity among sequentially passing droplets at high temporal resolution and sensitivity. Therefore, this approach paves a way toward hitherto impossible feedback control for handling, processing, and manipulating of droplets and their content in various high-throughput microfluidic units.

Utilizing the power of FCS for the study of periodically passing objects can facilitate and trigger a variety of additional applications where microscale objects are spatially arranged in solution due to flow, gravity, acoustic waves, or electromagnetic fields. Additionally, this approach enables the use of FCS for detecting and analyzing immobilized nanoscale objects patterned on a sliding specimen. Such a combination would provide high-throughput molecular readouts for binding assays and other in vitro analytical applications.

ASSOCIATED CONTENT

Supporting Information

The Supporting Information is available free of charge on the ACS Publications website at DOI: 10.1021/acs.analchem.7b03108.

Microfluidic device, importance of high sampling rate, generating droplets at different flow rates, marginal autofluorescence of the oil phase, monitoring cell encapsulations and droplets inhomogeneity at high temporal resolution, the droplet segmentation algorithm, segmentation and analysis of single droplets, detection of encapsulated cells in flowing droplets, input flow parameters of the aqueous and oil phases, interpretation of $G_D(\tau)$ amplitude (PDF)

DOI: 10.1021/acs.analchem.7b03108
Anal. Chem. 2017, 89, 11672−11678

AUTHOR INFORMATION

Corresponding Authors

*E-mail: eli.zamir@mpimf-heidelberg.mpg.de.
*E-mail: joachim.spatz@mpimf-heidelberg.mpg.de.

ORCID

Joachim P. Spatz: 0000-0003-3419-9807

Author Contributions

†(E.Z. and C.F.) These authors contributed equally.

Notes

The authors declare no competing financial interest.

ACKNOWLEDGMENTS

Parts of the research leading to these results have received funding from the European Research Council/ERC Grant Agreement no. 294852, SynAd. This work is also part of the MaxSynBio consortium, which is jointly funded by the Federal Ministry of Education and Research of Germany and the Max Planck Society. We thank Dr. Kerstin Goepfrich for helpful comments on the manuscript. The Max Planck Society is appreciated for its general support in all aspects of our research. The work was also partly supported by the SFB 1129 of the German Science Foundation and the VolkswagenStiftung (priority call "Life?"). J.P.S. is the Weston Visiting Professor at the Weizmann Institute of Science and part of the excellence cluster CellNetworks at the University of Heidelberg.

REFERENCES

(1) Bacia, K.; Kim, S. A.; Schwille, P. *Nat. Methods* **2006**, *3*, 83−89.
(2) Machan, R.; Wohland, T. *FEBS Lett.* **2014**, *588*, 3571−3584.
(3) Magde, D.; Elson, E. L.; Webb, W. W. *Biopolymers* **1974**, *13*, 29−61.
(4) Magde, D.; Webb, W. W.; Elson, E. *Phys. Rev. Lett.* **1972**, *29*, 705−708.
(5) Elson, E. L. *Biophys. J.* **2011**, *101*, 2855−2870.
(6) Sigaut, L.; Villarruel, C.; Ponce, M. L.; Ponce Dawson, S. *Phys. Rev. E: Stat. Phys., Plasmas, Fluids, Relat. Interdiscip. Top.* **2017**, *95*, 062408.
(7) Zamir, E.; Lommerse, P. H.; Kinkhabwala, A.; Grecco, H. E.; Bastiaens, P. I. *Nat. Methods* **2010**, *7*, 295−298.
(8) Pal, N.; Dev Verma, S.; Singh, M. K.; Sen, S. *Anal. Chem.* **2011**, *83*, 7736−7744.
(9) Gosch, M.; Blom, H.; Holm, J.; Heino, T.; Rigler, R. *Anal. Chem.* **2000**, *72*, 3260−3265.
(10) Haustein, E.; Schwille, P. *Methods* **2003**, *29*, 153−166.
(11) Guo, M. T.; Rotem, A.; Heyman, J. A.; Weitz, D. A. *Lab Chip* **2012**, *12*, 2146−2155.
(12) Joanicot, M.; Ajdari, A. *Science* **2005**, *309*, 887−888.
(13) Prakash, M.; Gershenfeld, N. *Science* **2007**, *315*, 832−835.
(14) Teh, S. Y.; Lin, R.; Hung, L. H.; Lee, A. P. *Lab Chip* **2008**, *8*, 198−220.
(15) Shembekar, N.; Chaipan, C.; Utharala, R.; Merten, C. A. *Lab Chip* **2016**, *16*, 1314−1331.
(16) Huebner, A.; Srisa-Art, M.; Holt, D.; Abell, C.; Hollfelder, F.; deMello, A. J.; Edel, J. B. *Chem. Commun. (Cambridge, U. K.)* **2007**, 1218−1220.
(17) Lu, H.; Caen, O.; Vrignon, J.; Zonta, E.; El Harrak, Z.; Nizard, P.; Baret, J. C.; Taly, V. *Sci. Rep.* **2017**, *7*, 1366.
(18) Pekin, D.; Taly, V. *Methods Mol. Biol.* **2017**, *1547*, 143−164.
(19) Sciambi, A.; Abate, A. R. *Lab Chip* **2015**, *15*, 47−51.
(20) Whitesides, G. M. *Lab Chip* **2010**, *10*, 2317−2318.
(21) Niu, X.; deMello, A. J. *Biochem. Soc. Trans.* **2012**, *40*, 615−623.
(22) Duffy, D. C.; McDonald, J. C.; Schueller, O. J. A.; Whitesides, G. M. *Anal. Chem.* **1998**, *70*, 4974−4984.
(23) Hofmann, T. W.; Hanselmann, S. H.; Janiesch, J. W.; Rademacher, A.; Bohm, C. H. J. *Lab Chip* **2012**, *12*, 916−922.
(24) Lisensky, G. C.; Campbell, D. J.; Beckman, K. J.; Calderon, C. E.; Doolan, P. W.; Ottosen, R. M.; Ellis, A. B. *J. Chem. Educ.* **1999**, *76*, 537.
(25) Platzman, I.; Janiesch, J.-W.; Spatz, J. P. *J. Am. Chem. Soc.* **2013**, *135*, 3339−3342.
(26) Holtze, C.; Rowat, A. C.; Agresti, J. J.; Hutchison, J. B.; Angile, F. E.; Schmitz, C. H. J.; Koster, S.; Duan, H.; Humphry, K. J.; Scanga, R. A.; Johnson, J. S.; Pisignano, D.; Weitz, D. A. *Lab Chip* **2008**, *8*, 1632−1639.
(27) Anna, S. L.; Bontoux, N.; Stone, H. A. *Appl. Phys. Lett.* **2003**, *82*, 364−366.
(28) Christopher, G. F.; Anna, S. L. *J. Phys. D: Appl. Phys.* **2007**, *40*, R319.
(29) Thorsen, T.; Roberts, R. W.; Arnold, F. H.; Quake, S. R. *Phys. Rev. Lett.* **2001**, *86*, 4163−4166.

DOI: 10.1021/acs.analchem.7b03108
Anal. Chem. 2017, 89, 11672−11678